SECED 2023 Conference
Earthquake Engineering & Dynamics for a Sustainable Future
14-15 September 2023, Cambridge, UK

IMPACT OF CORROSION DETERIORATION ON THE SEISMIC PERFORMANCE OF STEEL FRAME STRUCTURES

Devang LAD[1], Fabio FREDDI[2], Jayadipta GHOSH[3] & Tiziana ROSSETTO[4]

***Abstract**: Steel structures designed before the introduction of modern seismic design codes may be characterised by high seismic vulnerability due to their reduced ductility capacity. Additionally, these structures may be affected by significant corrosion deterioration, as one of the major atmospheric degradation phenomena when built in corrosive environments. Corrosion deterioration leads to a thickness reduction of sections, reduced bearing capacity, stiffness degradation and loss of energy dissipation capacity. Thus, old-corroded steel structures located in seismically active regions could experience a reduction of their seismic performance, significantly increasing the failure probability under earthquake events. The present study investigates the effect of atmospheric corrosion deterioration on steel frames and uses a non-seismically designed three-storey moment-resisting frame for case-study purposes. Atmospheric corrosion models based on the recommendation of ISO 9224:2012 have been adopted considering a 50-years ageing time and modelled as uniform corrosion on steel members. A probabilistic seismic performance assessment of the pristine and ageing steel frames is performed through Incremental Dynamic Analyses (IDAs). IDAs are performed for a set of 43 ground motion records accounting for the influence of the earthquake input's uncertainty (i.e., the record-to-record variability). The corrosion effects on the seismic performance are evaluated by monitoring both global and local engineering demand parameters (EDPs), allowing the development of seismic fragility functions at components- and system-level.*

***Keywords:** Steel moment resisting frame, Atmospheric corrosion, Existing structures, Fragility curves, Local engineering demand parameters.*

Introduction

Steel moment resisting frames (MRFs) represent a widely used structure typology in many seismic-prone regions worldwide. Many of these structures have been constructed before the introduction of modern seismic design codes and therefore are often characterised by a high seismic vulnerability due to inherent deficiencies typical of old design practices. Among others, the 1994 Northridge and 1995 Kobe earthquakes revealed numerous shortcomings in the design of such structures (Adey *et al*., 2000; Mahin, 1998), including the absence of capacity design, weak panel zones, brittle welding zones, low ductility, inadequate energy dissipation capacity, *etc.* (Gutiérrez-Urzúa *et al.*, 2021).

In addition, existing steel structures are often characterised by corrosion deterioration which may further compromise their seismic performance (Li and Mahmoodian, 2022). A few studies highlighted how corrosion can adversely reduce strength and ductility of steel MRFs, making them more vulnerable to structural damage under seismic events (Di Sarno *et al.*, 2021). The primary effects include the reduction in the thickness of steel sections due to the formation of rust, while the secondary effects include the reduction of material properties (*i.e.,* yield and ultimate strength, ductility, modulus of elasticity) (Wang *et al.*, 2018). Nowadays, a large amount of research studies is focusing on assessing corrosion's impact on the seismic performance of bridge structures and infrastructures (*e.g.,* Ghosh and Sood, 2016; Shekhar *et al.*, 2018). On the contrary, only a few research works have investigated the combined impact of corrosion deterioration and earthquakes on existing steel buildings.

[1] PhD Student, University College London, London, United Kingdom, devang.lad.21@ucl.ac.uk
[2] Lecturer, University College London, London, United Kingdom
[3] Associate Professor, Indian Institute of Technology Bombay, Mumbai, India
[4] Professor, University College London, London, United Kingdom

Zhang *et al.* (2020) experimentally and numerically investigated the seismic response of a three-storey single-bay MRF by considering different levels of corrosion. The results showed that a corrosion mass loss of 10.13% resulted in significant reductions in global displacement ductility and base shear capacity. Di Sarno *et al*. (2021) numerically investigated the seismic performance of a high-rise steel building considering a C4 corrosivity category (defined as per ISO 9224: 2012 guidelines) for a 100-year period. The results showed that the seismic response of the structure in terms of storey drifts is significantly increased when compared with C3 and C2 categories. These and a few other numerical studies investigated the response of corroded steel structures; however, in most cases, the contribution of corrosion at beam-to-column joint modelling has been neglected. In addition, most of the studies focused on the global response of corroded structures while, to the authors knowledge, no research study investigated the impact of corrosion at components level (*e.g.,* beams, columns, panel zones, connections).

In order to fill these knowledge gaps, the present study investigates the seismic performance of a low-rise steel building designed as per pre-Northridge seismic codes and evaluates the impact of atmospheric corrosion deterioration. A three-storey steel MRF, adopted from the SAC-FEMA project (Gupta, 1999), is considered for case-study purposes. The joints are considered welded as per the original data available. The structure is assumed to be exposed to atmospheric conditions of the coastal area for a 50-years period. The time-dependent atmospheric corrosion deterioration model is adopted as suggested by ISO 9224: 2012. Uniform corrosion is considered for columns and panel zones, together with the deterioration in the mechanical properties of steel. A finite element (FE) model of the frame is developed in OpenSees (McKenna *et al*., 2000) to carry out non-linear static and dynamic numerical simulations. The study also investigates the probabilistic seismic response of the pristine and ageing steel frames through Incremental Dynamic Analyses (IDAs), considering a set of 43 ground motion records to account for the influence of the record-to-record variability. The seismic performance is assessed at global- and component-level by monitoring the relevant engineering demand parameters (*EDPs*). Seismic fragility functions at system- and components-level are finally developed to evaluate and critically discuss on the influence of corrosion effect on the global and local level seismic performance of the steel frame.

Methodology

Figure 1 shows the overall framework used in the present study for fragility assessment of the case-study steel MRF.

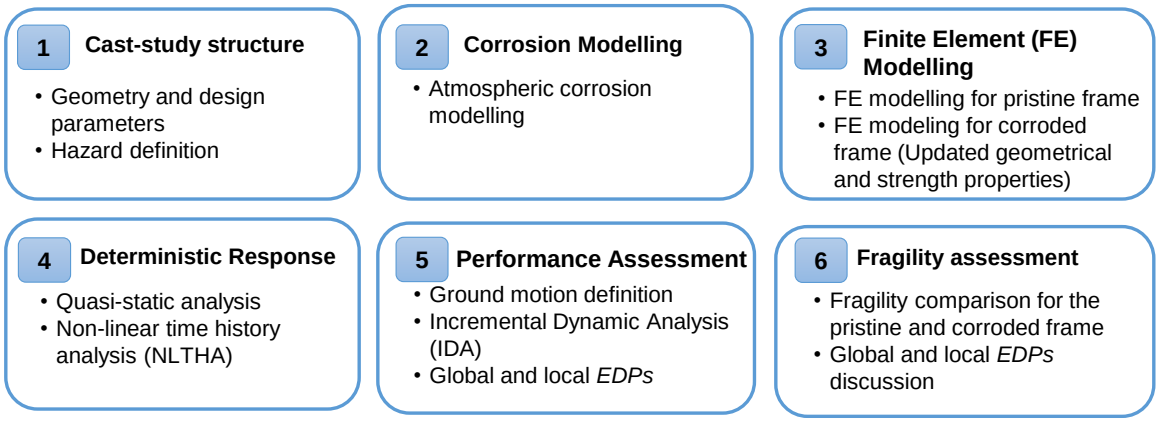

Figure 1. Seismic fragility assessment framework for corroded steel moment resisting frames (MRFs).

In Step 1, the benchmarked steel building is selected, and the details of the building and site under consideration are provided. Step 2 introduces corrosion deterioration in steel frames together with the models used to estimate atmospheric corrosion deterioration. In Step 3, FE models of the pristine and corroded frames are developed in OpenSees (McKenna *et al*., 2000) by incorporating the primary and secondary deterioration effects. In Step 4, the lateral strength of the pristine *vs.* the corroded frame is compared using displacement-controlled quasi-static analysis. The local and global *EDPs* of interest are discussed together with their capacity limit states and the Intensity Measure (*IM*) used in this study. Also, non-linear time history analyses for a single ground motion record are performed on the pristine and corroded frames to provide

some indication of the effects of corrosion on the seismic response at global- and components-level. In Step 5, IDAs for the chosen suite of ground motion records are performed on the pristine and corroded frames to evaluate their response parameters considering the influence of the record-to-record variability. Finally, in Step 6, fragility assessment for the pristine and corroded frames is evaluated and compared.

Case-study structure, corrosion deterioration and Finite Element (FE) modelling

Case-study structure

Boston's three-storey building (3B) from the SAC-FEMA project is adopted as case-study structure (Gupta, 1999). This frame was designed according to the 12th edition of the National Building Code, considered built on stiff soil with regular floor plan distribution, and steel grade ASTM A572. The case-study structure represents typical low-rise structures designed using non-seismic pre-Northridge design codes (Gupta, 1999), does not incorporate capacity-based design considerations and is characterised by low-ductile joints. The plan and elevation views of the structure are shown in Figure 2. The perimeter seismic-resistant steel MRF considered in this study is represented by the thick lines in Figure 2(a), while its elevation view is shown in Figure 2(b). This MRF has a bay width of 9144 mm and an interstorey height of 3962 mm. Columns' and beams' sections are indicated in Figure 2(b). The seismic masses for the 1st, 2nd, and 3rd storey are 956.6, 956.6, and 1035 tons, respectively. Only half of each storey mass is assigned in the FE model for a single perimeter frame (*i.e.,* two perimeter MRFs in the *x*-direction). The seismic risk category II (*e.g.*, small office building), according to ASCE 7-16, is adopted for the case-study structure. Additional details regarding the case-study structure are provided by Gutiérrez-Urzúa *et al*. (2021) and Gutiérrez-Urzúa and Freddi (2022).

The case-study structure is assumed to be located near Boston's coastline in an urban area with medium pollution exposure, corresponding to the C4 (high) corrosivity category according to ISO 9223: 2012. In addition, it is assumed that no protection in the form of paint is applied to the case-study structure. The analysis considers the structure as pristine and with a 50-year ageing period.

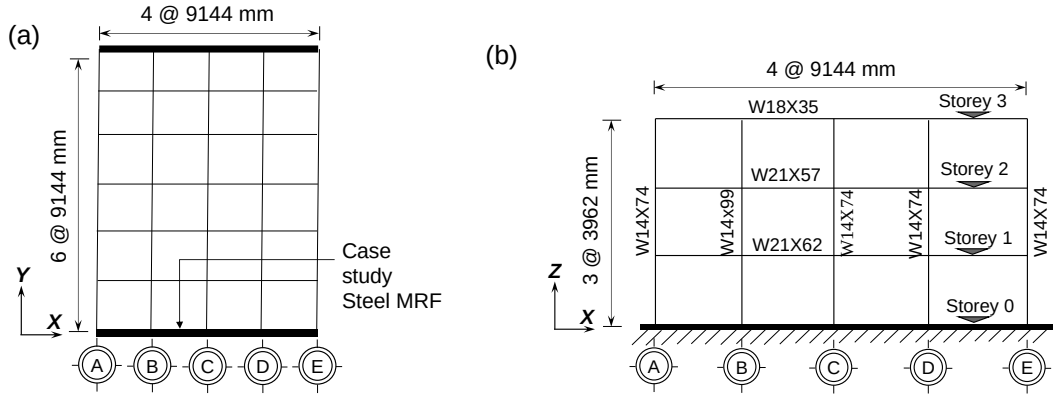

Figure 2. Case-study steel moment-resisting frame (MRF): (a) Plan view; (b) Elevation view.

Atmospheric corrosion deterioration modelling

Atmospheric corrosion is an electrochemical reaction in a steel member resulting in thickness loss on the entire surface or locally. The potential difference causes electron loss from the base steel metal to form the corrosion product, *i.e.,* rust (Buchanan and Stansbury, 2012). Corrosion deterioration in steel structures includes uniform corrosion, pitting corrosion, fatigue corrosion, stress-induced corrosion, and many more (Di Sarno *et al*., 2021).

Corrosion deterioration causes thickness loss of steel section and degradation of the steel's mechanical properties. The deterioration over a period of time is typically modelled using the corrosion rate (i_{corr}) in μm/year, which subsumes the complex relationships between environmental factors of the corrosion phenomena. Thus, ISO 9223: 2012 provides the following factors to classify the atmosphere for corrosion of metals: (1) temperature-humidity complex, (2) sulphur dioxide, and (3) chloride pollution. As previously stated, this study adopts the C4 corrosivity category for atmospheric corrosion characteristics from ISO 9223: 2012.

To estimate the thickness loss due to corrosion deterioration, this study adopts the corrosion loss model from ISO 9224: 2012. This is defined by a discontinuous function for ageing periods shorter and longer than 20 years according to the following formulation:

$$d(t \leq 20y) = i_{corr} t^{B}$$
$$d(t > 20y) = i_{corr}[20^{B} + B(20^{B-1})(t - 20)] \quad (1)$$

where the value of i_{corr} is the first-year corrosion rate, B is the time exponent coefficient and $d(t)$ is the cross-section thickness loss of steel member (in μm). ISO 9224: 2012 suggest that power law is valid up to 20 years, assuming that the increasing rust thickness alleviates the corrosion damage. Furthermore, for post 20-year ageing time, it assumes that the corrosion achieves a steady state with a linear corrosion rate. The values of i_{corr} and B for the C4 corrosivity category are taken as the average of the limits provided in ISO 9224: 2012, which are i_{corr} = 65 $\mu m/year$ and B = 0.575 for carbon steel. Adopting these values, the thickness loss for 50 years is $d(t = 50y)$ = 0.55 mm on the exposed side, corresponding to a mass loss of 6.8%.

Furthermore, degradation in steel's mechanical properties is evaluated based on the degrading laws proposed by Wang *et al*. (2018). The modified properties are calculated based on corrosion mass loss, given according to the following formulation:

$$f_y = f_{yo}(1 - 1.09\eta) \quad (2)$$

$$f_u = f_{uo}(1 - 1.07\eta) \quad (3)$$

where f_{yo} and f_{uo} are initial yield and ultimate strength of the material, while η is the mass loss ratio. For a mass loss ratio (η) of 6.8%, f_{yo} and f_{uo} are reduced by a factor of 0.92.

Finite element (FE) modelling

A 2D non-linear FE model of the case-study structure is developed in OpenSees (McKenna *et al*., 2000). Columns are modelled using a distributed plasticity approach to account for the interaction between axial and bending stresses. Conversely, beams are modelled according to a lumped plasticity approach. The properties of the beams' plastic hinges are calibrated and modified as per the model proposed by Lignos and Krawinkler (2011) and Zareian and Medina (2010), respectively. In addition, panel zones are modelled as per the 'Scissors model' using two parallel rotational springs (Gutiérrez-Urzúa *et al*., 2021). Beam-to-column connections are assumed welded and therefore are considered rigid in the FE model. The yield strength (f_y) and elastic modulus (*E*) are respectively equal to f_y= 344.74 MPa and *E* = 199.95 GPa. ASCE 41-17 recommends increasing the nominal value of f_y by 10% to account for the material overstrength. A damping ratio of ζ = 3% is adopted by using mass and stiffness proportional damping (*i.e.,* Rayleigh Damping). Additionally, a leaning column is included in the model to account for the P-Δ effects generated by the loads applied on the gravity frame. Additional information on the FE model are provided in Gutiérrez-Urzúa *et al*. (2021).

For the 50-year frame, thickness loss due to atmospheric corrosion deterioration is considered for all columns. The column sections in the FE model are revised to account for the thickness loss calculated as per Eq. (1) ($d(t)$=0.55 mm). The rotational spring properties modelled as per 'Scissors model' is revised based on $d(t = 50y)$ for column sections. Degradation in the mechanical properties is accounted for by modifying the yield (f_y) and ultimate strength (f_u) as per Eq. (2) and Eq. (3). A schematic representation of thickness loss in the column section for uniform corrosion along the full length is shown in Figure 3(a). The components in the corroded frame incorporating uniform corrosion are shown in Figure 3(b). In this study, no deterioration is considered for beams as they typically support and are partially protected by the slab, are located in the interior region of the building, and thus are in a less corrosive environment. Moreover, being non-seismically designed and characterised by weak panel zones, beam deterioration has a negligible impact on the lateral strength of the considered case-study frame.

Seismic performance assessment

Engineering Demand Parameters (EDPs) and code-based capacity limits

Local and global *EDPs* are used to evaluate the seismic performance of the case-study structure, also accounting for the corrosion effects. The considered local *EDPs* include the beams' chord rotation (θ_b), column' chord rotation (θ_c), and panel zone shear strain (γ). On the other end, the

considered global *EDP* is the maximum interstorey drift ratio (*MIDR*), which provides a synthetic description of the seismic response.

Capacity limits for the considered local *EDPs* are conventionally defined based on yield capacity parameters, which for beams and columns is represented by the chord rotation at yielding (θ_y), while for panel zones is represented by the shear yield strain (γ_y). Table 1, as per ASCE 41-17, describes the yield capacity parameters for beams, columns, and panel zones in terms of θ_y. The coefficient, $\mathrm{Z} = M_{pb,Rd}L\,/\,6EI$ in Table 1, where $M_{pb,Rd}$ is the plastic moment capacity of the element at the location of the plastic hinge, *L* is the span's length (for beams) or column's height (for columns), while E and I are the Young's modulus and moment of inertia of the element, respectively. Additionally, in Table 1, G is the shear modulus of steel, A_s is the effective shear area of the cross-section, and $\nu_G = N_G/N_{pl,Rd}$ is the dimensionless gravity force where N_G is axial force demand and $N_{pl,Rd}$ axial capacity of the element.

For these *EDPs*, the ASCE 41-17 provides three different limit states (*LSs*), namely the (1) Immediate Occupancy (*LS1*), (2) Life Safety (*LS2*), and (3) Collapse Prevention (*LS3*). For beams, the capacity limits (*i.e., LSs* thresholds) are defined only in terms of plastic rotation thresholds and slenderness characteristics of the web and flanges of the cross-section. Conversely, in columns, the influence of axial loads is also considered, the plastic rotation capacity is decoupled from θ_y , and described in terms of ductility parameters a and b , respectively, as defined in ASCE 41-17 (Gutiérrez-Urzúa *et al*., 2021). For the considered case-study structure, all columns are characterised by a dimensionless axial load $\nu_G \leq 0.6$. For columns with high axial load ($\nu_G > 0.6$), the limit states are force-controlled, and details can be found in Gutiérrez-Urzúa *et al.* (2021). Finally, for panel zones, the deformation capacity limits are given in terms of yield shear strain (γ_y) or the corresponding rotation (θ_y). The details of these capacity limits are summarized in Table 2. Additionally, the capacity limits for the *MIDR* are assumed equal to 0.7% (*LS1*), 2.5% (*LS2*), and 5% (*LS3*) according to the ASCE 41-07.

Beams	**Columns**	**Panel zones**
$\theta_y = \mathrm{Z}\left(1 + \frac{12EI}{L^2GA_s}\right)$	$\theta_y = \begin{cases} \nu_G \leq 0.2, & \mathrm{Z}\left(1 + \frac{12EI}{L^2GA_s}\right)\left(1 - \frac{\nu_G}{2}\right) \\ 0.2 < \nu_G \leq 0.5, & \mathrm{Z}\left(1 + \frac{12EI}{L^2GA_s}\right)\left(\frac{9}{8} - \frac{9\nu_G}{8}\right) \end{cases}$	$\theta_y = \frac{f_{ye}}{G\sqrt{3}}\sqrt{1 - \nu_G^2}$

Table 1. Deformation-based yield capacity parameters for beams, column and panel zones as per ASCE 41-17.

Element	**Dimensionless axial load limits**	**Slenderness limits***	**Plastic rotation capacity limits**		
			LS1	***LS2***	***LS3***
Beams**	-	$\alpha \leq 1123$ & $\beta \geq 171$	2.25 θ_y	9 θ_y	11 θ_y
	-	Intermediate values		Interpolate	
	-	$\alpha \leq 1723$ & $\beta \geq 174$	1 θ_y	3 θ_y	4 θ_y
Columns***	$\lvert\nu_G\rvert \leq 0.6$	All	0.5 a	$0.75b$	b
Panel Zone	$\lvert\nu_G\rvert < 0.4$	-	1 θ_y	12 θ_y	12 θ_y

***Notes**:* *Interpolation must be made between web and flange slenderness limits, and the lowest rotation limits should be taken for each limit state*;* ** The slenderness limit parameter for web - $\alpha = (h/t_w) \times \sqrt{f_y}$, and for flange - $\beta = (b_f/2t_f)\sqrt{f_y}$; *** The terms '$a$' and '$b$' are defined in Table 9-7.1 of the ASCE 41-17.

Table 2. Component-level plastic rotation capacity limit states as per ASCE 41-17.

Intensity Measure (IM)

A reduction in the section thickness due to corrosion deterioration typically generates a slight stiffness reduction and a consequent period elongation of the corroded frame with respect to the pristine frame. Thus, in order to allow the comparison of the seismic response of the two frames, the average spectral acceleration ($S_{a,avg}$) between the fundamental time periods of the pristine ($T_{1,p}$) and corroded ($T_{1,c}$) frames is used as *IM* in this study. This can be defined as the geometric mean of accelerations between $T_{1,p}$ and $T_{1,c}$, according to the following formulation:

$$S_{a,avg}\left(T_{1,p} - T_{1,c}, \zeta = 3\%\right) = \left(\prod_{i=1}^{n} S_a(T_{1,n})\right)^{1/n} \quad (4)$$

where n is the number of discrete spectral ordinates between $T_{1,p}$ and $T_{1,c}$. The adopted $S_{a,avg}$ allows directly comparing the fragility curves for the pristine and corroded frames.

Quasi-static analysis

Non-linear quasi-static analysis with the distribution of lateral loads defined according to the first mode is performed to assess the lateral strength for the pristine and 50-year corroded frames. Figure 3(c) shows the response of the pristine and corroded frames in terms of base shear *vs.* first-storey interstorey drift ratio (*IDR*). The lateral strength in terms of base shear for the 50-year corroded frames reduces by approximately 17% with respect to the pristine frame. In addition, a minor stiffness loss is also observed, leading to a slight fundamental period elongation, *i.e.,* $T_{1,p}$ =1.88 sec and $T_{1,c}$ =1.92 sec.

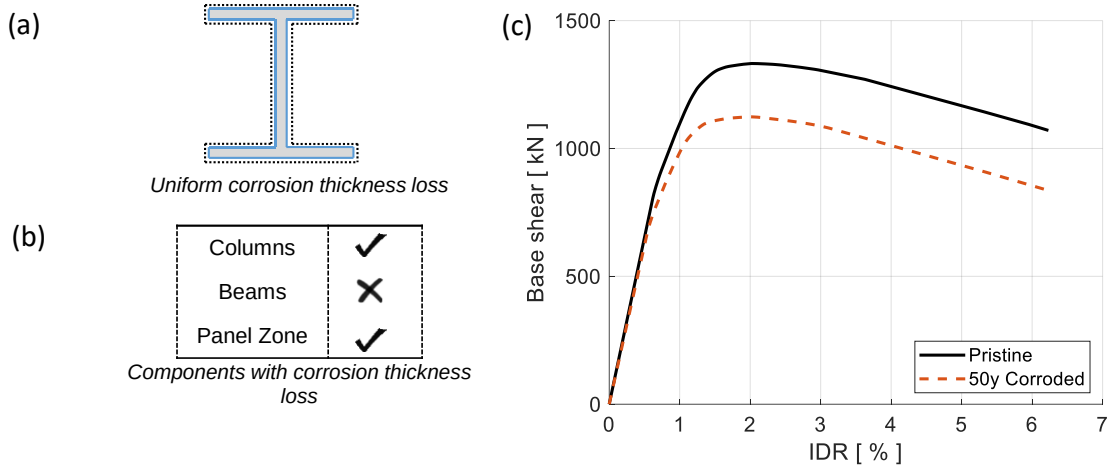

Figure 3. (a) Representative of column cross-section due to corrosion deterioration; (b) Description of component level corrosion considerations; (c) Non-linear quasi-static analysis of the pristine and corroded frame- Base shear vs. Interstorey Drift Ratio for the 1st storey.

Non-linear time history analysis

The response of the non-linear time history analyses of the pristine and corroded frames under a single ground motion (GM) record is presented in this section. Figure 4(a) shows the first-storey drift response for a single GM record scaled to 0.2g of the *IM* for the pristine and corroded frames. Figure 4(a) highlights that, in this case, corrosion deterioration causes approximately 14% higher maximum interstorey drift (IDR_{max}) and 74% higher residual interstorey drift (IDR_{res}) in the first-storey. Figure 4(b) shows the normalised rotation with respect to its yielding value (θ/θ_y) for panel zone no 7 (PZ 7). It highlights that PZ 7 has reached the plastic deformation stage for both the pristine frame and corroded frames. However, the PZ 7 of the corroded frame under seismic loads observe significantly larger rotation compared to the pristine frame.

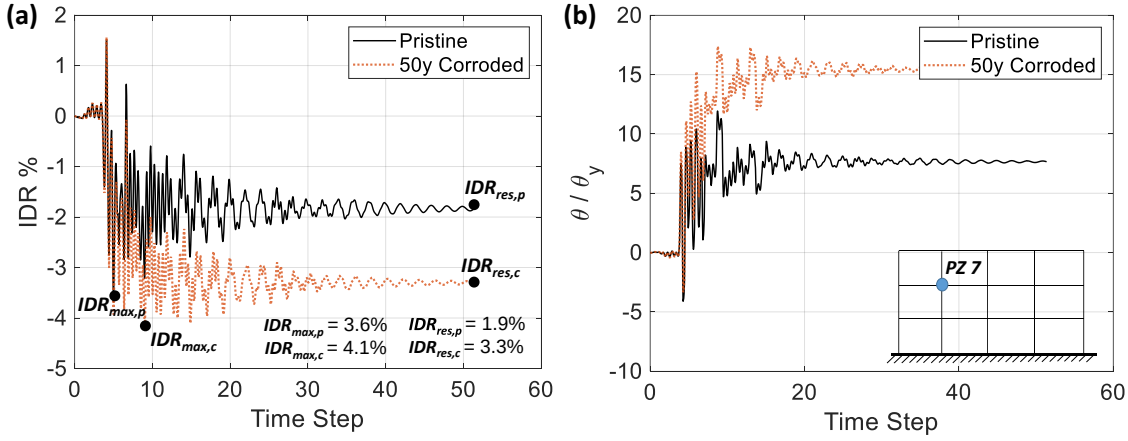

Figure 4. Time history response for pristine and corroded frames (a) first-storey IDR (%) and (b) normalised rotation of panel zone PZ 7 (θ/θ_y).

Incremental Dynamic Analyses (IDAs) and Fragility Curves

A suite of 43 far-field GM records developed for the ATC-63 project (FEMA, 2009) was used to perform IDAs. The GMs were recorded on stiff soil, and do not exhibit pulse-type characteristics

(*i.e.,* source-to-site distance larger than 10 km). These GMs are not site-specific; thus, this study intends to assess the seismic performance representing a generalized seismic hazard. The selected GMs are scaled to different *IM* values ranging from 0.1g to 1g. IDAs for the GMs suite provide samples of the demand for the selected *EDPs* for discrete *IM* values.

Based on the *EDPs-IM* pairs, fragility curves are successively derived for the local- and global-level *EDPs* discussed in the previous sections. Fragility curves provide the probability of exceeding a specified *LS*, conditional to the strong-motion shaking severity, quantified by an appropriately selected *IM*. For each type of *EDPs* considered (*i.e.,* beams' chord rotation - θ_b, column' chord rotation - θ_c, panel zone shear strain – γ, and MIDRs), and for each GM, the maximum response monitored among all components is considered as sample of the demand (*i.e.,* series arrangement of the components) (Freddi *et al*., 2013). On the other end, the code-based capacity limits (ASCE 41-17) discussed in the previous sections are used for comparison with the demand values and hence, for the definition of fragility curves. In other words, fragility curves for each *EDP* type and for the whole set of GMs are derived based on the comparison of the maximum *EDP* values among all components with respect to the capacity limit.

While accounting for the uncertainty in seismic demand (*i.e.,* record-to-record variability), the variation of demand-dependent and deterioration-dependent capacity values is implicitly considered in this study (*i.e.,* θ_y in beams, columns, and panel zones). Other sources of uncertainty are neglected in this study. The deterioration-dependent capacity variation is based on the θ_y values, which are function of yield (f_y) and ultimate (f_u) strength of the material and of the geometry of the section (*i.e.,* thickness of web and flanges) at a point in time. As per the equations in Table 1, Z parameter is a function of f_y where the reduction in f_y and the reduction in the web and flanges thickness due to corrosion deterioration, leads to reduction in rotation capacity.

Numerical fragility curves are derived based on the direct comparison between the samples of the demand and the corresponding capacity limits for each *EDP*. Successively, numerical fragility curves are approximated by analytical lognormal curves obtained through least-square minimization. The component-level seismic fragility curves can be described as follows:

$$P(DS > LS|IM) = P(\theta > n_{LS}\theta_y|IM) \quad (5)$$

where θ represents the demand value, while $n_{LS}\theta_y$ represents the capacity limit for each *EDP* and each *LS*, estimated separately for pristine and corroded frames. Global fragility curves are derived in a similar way but without accounting for the evolution of the capacity limit values due to corrosion. Figure 5 provides the fragility curve for the pristine and corroded frame for both global and local *EDPs*. At the same time, for an easier comparison of the results, Table 3 reports the median (med) of the lognormal fragility curves for the pristine and corroded frames and their percentile variations.

Figure 5(a) shows the fragility curves for the *MIDR*. It can be observed that there is a small difference between the pristine and corroded frames for *LS1* and *LS2*. Conversely, for *LS3* the corroded frame shows a higher fragility with a difference in terms of median value of the lognormal fragility curves (med) of 8.9% (see Table 3). Figure 5(b) shows the fragility curves for beam's chord rotation (θ_b). In this case, a small variation with a slightly reduced fragility is observed for the *LS1* of the corroded compared to the pristine frame. Conversely, a significant increase of fragility exists for both *LS2* and *LS3* with percentage variations of med values respectively equal to 14.6% and 14.1% (see Table 3). Figure 5(c) shows the fragility curves for column' chord rotation (θ_c). In this case, increased fragilities are observed for all *LSs*. The fragility for *LS1* shows the highest increase with a percentage variation of the med value of 17.4%. Fragilities for LS2 and LS3 show variations of med values, respectively of 13.2% and 12.5% (see Table 3). Figure 5(d) shows the fragility curves for panel zone shear rotations (θ). Also in this case, increased fragilities are observed for all *LSs* with med values of the corroded frame 9.3%, 6.3%, and 6.3% lower than the pristine frame for the *LS1*, *LS2* and *LS3*, respectively (see Table 3). It is worth reminding the reader that, for this component, the ASCE 41-17 provides the same definition of capacity limits for *LS2* and *LS3,* and for this reason, the fragility curves coincide.

Comparing the fragilities of beams, columns, and panel zone rotations in Figure 5, it can be observed that the panel zone is the weakest component for all *LSs*. Thus, the panel zone under seismic action and corrosion deterioration governs the whole frame's exceedance probability. However, this component shows the lowest fragility variation as a consequence of the corrosion

effects. On the other side, columns represent the components with the highest increase in fragility, potentially leading to a change of failure modalities for longer ageing periods.

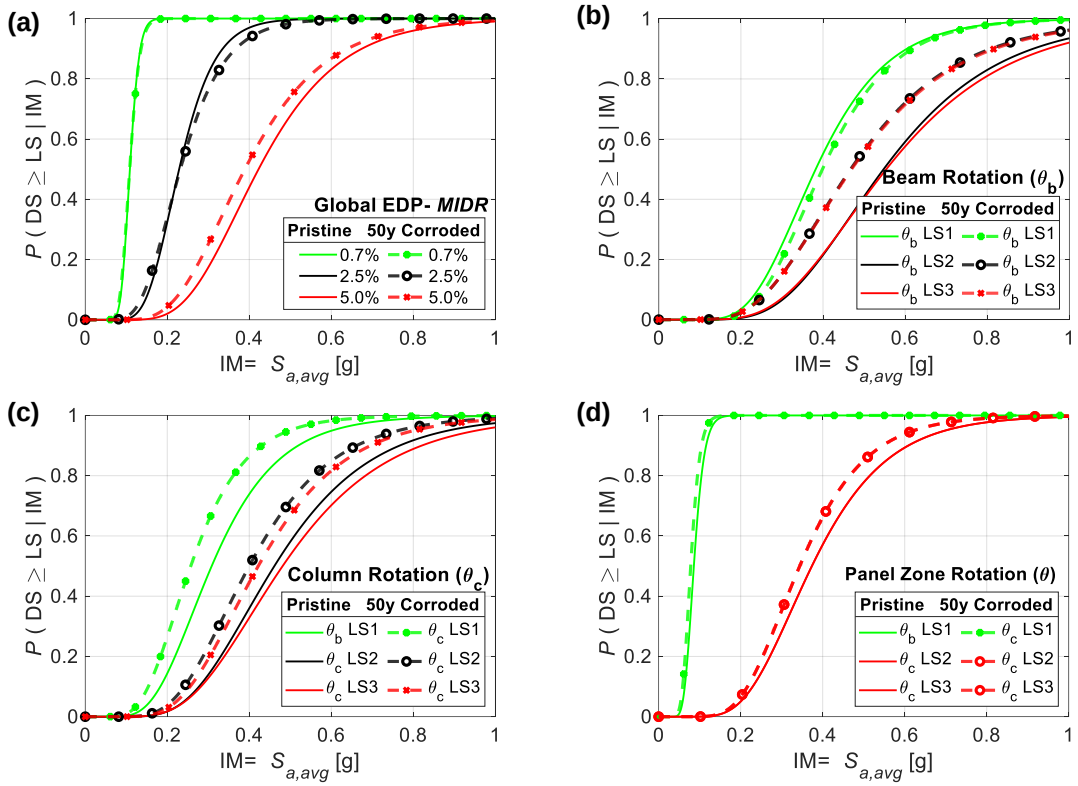

Figure 5. Fragility curves for the case-study structure (3B) for (a) global EDPs (i.e., MIDR) and local EDPs - (b) beam rotation (θ_b), (c) column rotation (θ_c), and (d) panel zone rotation (θ).

Frames	MIDRs			Beams			Columns			Panel Zones		
	LS1	*LS2*	*LS3*	*LS1*	*LS2*	*LS3*	*LS1*	*LS2*	*LS3*	*LS1*	*LS2*	*LS3*
Pristine	0.109	0.227	0.427	0.382	0.547	0.547	0.311	0.461	0.481	0.086	0.367	0.367
Corroded	0.108	0.232	0.389	0.399	0.467	0.470	0.257	0.400	0.421	0.078	0.344	0.344
% var.	*0.9%*	*-2.2%*	*8.9%*	*-4.5%*	*14.6%*	*14.1%*	*17.4%*	*13.2%*	*12.5%*	*9.3%*	*6.3%*	*6.3%*

Table 3. Median (med) of the lognormal fragility curves for pristine and corroded frames.

Conclusions

Steel structures designed before the introduction of modern seismic design codes may be characterised by high seismic vulnerability due to their reduced ductility capacity. Additionally, these structures may be affected by significant corrosion deterioration, as one of the major atmospheric degradation phenomena when built in corrosive environments. The present study investigates the seismic performance of a non-seismically designed existing steel moment resisting frame (MRF) under the influence of atmospheric corrosion deterioration for a 50-years ageing time. A finite element (FE) model in OpenSees was developed to simulate the seismic response of the case-study structure through non-linear quasi-static and dynamic analyses. This study considers global (*i.e.*, maximum interstorey drifts - MIDR), and local engineering demand parameters (*EDPs)* (*i.e.,* beams' chord rotation - θ_b, column' chord rotation - θ_c, panel zone shear strain – γ), to evaluate the seismic performance of the frame after corrosion deterioration. Atmospheric corrosion's primary and secondary effects were quantified based on the recommendations of ISO 9224:2012 and incorporated in the FE model as uniform corrosion on steel members. The primary effect of atmospheric corrosion leads to a mass loss of the cross-section due to rust formation. For the 50-year exposure time and C4 corrosivity category (high), a 6.8% mass loss was estimated. The secondary effect includes the reduction of yield strength (f_y) and ultimate strength (f_u) of steel and were estimated to be about 8%. The results of the quasi-static analysis revealed a significant reduction (*i.e.,* approximately 17%) in the lateral strength of the structure due to corrosion effects. Conversely, only a minor reduction in the stiffness of the case-study frame was observed. Incremental Dynamic Analyses (IDAs) were

successively performed for a set of 43 ground motion records to assess the seismic performance of the structure accounting for the influence of the earthquake input's uncertainty and to derive fragility curves. Fragility curves have been derived for both global- and local-level *EDPs* considering code-based capacity limits for three different limit states (*LS*s). The fragility assessment highlighted that panel zones represent the weakest components in both the pristine and corroded scenarios. However, these components show the lowest fragility variation as a consequence of the corrosion effects (*i.e.,* up to 9.3%). On the other side, columns represent the components with the highest increase in fragility (*i.e.,* up to 17.4%). This situation could potentially lead to a change of failure modalities of the structure for longer ageing periods. The results of this study shed some light on the influence of corrosion deterioration of steel MRFs and provide some preliminary results for the quantification of the seismic fragility increase due to corrosion. Future works will investigate the effects of pitting corrosion and stress-induced corrosion at welded and bolted joints, the influence of modelling uncertainties related to the corrosion effects, and will extend the study to additional case-study structures to generalise the results.

References

Adey, B.T., Grondin, G.Y., Cheng, J.J.R., 2000. Cyclic loading of end plate moment connections 27.

American Society of Civil Engineers, 2017. Minimum Design Loads and Associated Criteria for Buildings and Other Structures, ASCE/SEI 7-16. ed. American Society of Civil Engineers. https://doi.org/10.1061/9780784414248

American Society of Civil Engineers, 2007. Seismic Rehabilitation of Existing Buildings, ASCE/SEI 41-06. ed. American Society of Civil Engineers. https://doi.org/10.1061/9780784408841

Buchanan, R.A., Stansbury, E.E., 2012. Electrochemical Corrosion, in: Handbook of Environmental Degradation of Materials. Elsevier, pp. 87–125. https://doi.org/10.1016/B978-1-4377-3455-3.00004-3

Di Sarno, L., Majidian, A., Karagiannakis, G., 2021. The Effect of Atmospheric Corrosion on Steel Structures: A State-of-the-Art and Case-Study. Buildings 11, 571. https://doi.org/10.3390/buildings11120571

FEMA, P. 695, 2009. Quantification of building seismic performance factors.

Freddi, F., Tubaldi, E., Ragni, L., Dall'Asta, A., 2013. Probabilistic performance assessment of low-ductility reinforced concrete frames retrofitted with dissipative braces: Seismic Performance Of Low-Ductility Rc Frames With Dissipative Braces. Earthquake Engng Struct. Dyn. 42, 993–1011. https://doi.org/10.1002/eqe.2255

Ghosh, J., Sood, P., 2016. Consideration of time-evolving capacity distributions and improved degradation models for seismic fragility assessment of aging highway bridges. Reliability Engineering & System Safety 154, 197–218. https://doi.org/10.1016/j.ress.2016.06.001

Gupta, A., 1999. Seismic demands for performance evaluation of steel moment resisting frame structures. Stanford University.

Gutiérrez-Urzúa, F., Freddi, F., 2022. Influence of the design objectives on the seismic performance of steel moment resisting frames retrofitted with buckling restrained braces. Earthq Engng Struct Dyn 51, 3131–3153. https://doi.org/10.1002/eqe.3717

Gutiérrez-Urzúa, F., Freddi, F., Di Sarno, L., 2021. Comparative analysis of code-based approaches for seismic assessment of existing steel moment resisting frames. Journal of Constructional Steel Research 181, 106589. https://doi.org/10.1016/j.jcsr.2021.106589

ISO 9223: 2012, 2012. Corrosion of metals and alloys—corrosivity of atmospheres—classification, determination and estimation. The British Standard Institute.

ISO 9224: 2012(E), 2012. Corrosion of Metals and Alloys – Corrosivity of Atmospheres – Guiding Values for the Corrosivity Categories. International Standards Organization, Geneve.

Li, L., Mahmoodian, M., 2022. Fatigue Life Prediction And Maintainance Management Of Steel Structures Subjected To Corrosion. Australian Journal of Structural Engineering 23, 75–88. https://doi.org/10.1080/13287982.2021.1999041

Lignos, D.G., Krawinkler, H., 2011. Deterioration Modeling of Steel Components in Support of Collapse Prediction of Steel Moment Frames under Earthquake Loading. J. Struct. Eng. 137, 1291–1302. https://doi.org/10.1061/(ASCE)ST.1943-541X.0000376

Mahin, S.A., 1998. Lessons from damage to steel buildings during the Northridge earthquake. Engineering Structures 20, 261–270. https://doi.org/10.1016/S0141-0296(97)00032-1

McKenna, F., Fenves, G.L., Scott, M.H., others, 2000. Open system for earthquake engineering simulation. University of California, Berkeley, CA.

Shekhar, S., Ghosh, J., Padgett, J.E., 2018. Seismic life-cycle cost analysis of ageing highway bridges under chloride exposure conditions: modelling and recommendations. Structure and Infrastructure Engineering 14, 941–966. https://doi.org/10.1080/15732479.2018.1437639

Wang, H., Xu, S., Li, A., Kang, K., 2018. Experimental and numerical investigation on seismic performance of corroded welded steel connections. Engineering Structures 174, 10–25. https://doi.org/10.1016/j.engstruct.2018.07.057

Zareian, F., Medina, R.A., 2010. A practical method for proper modeling of structural damping in inelastic plane structural systems. Computers & Structures 88, 45–53. https://doi.org/10.1016/j.compstruc.2009.08.001

Zhang, X., Zheng, S., Zhao, X., 2020. Experimental and numerical study on seismic performance of corroded steel frames in chloride environment. Journal of Constructional Steel Research 171, 106164. https://doi.org/10.1016/j.jcsr.2020.106164